JACS
JOURNAL OF THE AMERICAN CHEMICAL SOCIETY
Article
pubs.acs.org/JACS

Ion-Exchangeable Molybdenum Sulfide Porous Chalcogel: Gas Adsorption and Capture of Iodine and Mercury

Kota S. Subrahmanyam,[†] Christos D. Malliakas,[†] Debajit Sarma,[†] Gerasimos S. Armatas,[§] Jinsong Wu,[‡] and Mercouri G. Kanatzidis*[,†]

[†]Department of Chemistry and [‡]Department of Materials Science and Engineering, NUANCE Center, Northwestern University, 2145 Sheridan Road, Evanston, Illinois 60208, United States

[§]Department of Materials Science and Technology, University of Crete, Heraklion 71003, Crete, Greece

Supporting Information

ABSTRACT: We report the synthesis of ion-exchangeable molybdenum sulfide chalcogel through an oxidative coupling process, using $(NH_4)_2MoS_4$ and iodine. After supercritical drying, the MoS_x amorphous aerogel shows a large surface area up to 370 m^2/g with a broad range of pore sizes. X-ray photoelectron spectroscopic and pair distribution function analyses reveal that Mo^{6+} species undergo reduction during network assembly to produce Mo^{4+}-containing species where the chalcogel network consists of $[Mo_3S_{13}]$ building blocks comprising triangular Mo metal clusters and S_2^{2-} units. The optical band gap of the brown-black chalcogel is ~1.36 eV. The ammonium sites present in the molybdenum sulfide chalcogel network are ion-exchangeable with K^+ and Cs^+ ions. The molybdenum sulfide aerogel exhibits high adsorption selectivities for CO_2 and C_2H_6 over H_2 and CH_4. The aerogel also possesses high affinity for iodine and mercury.

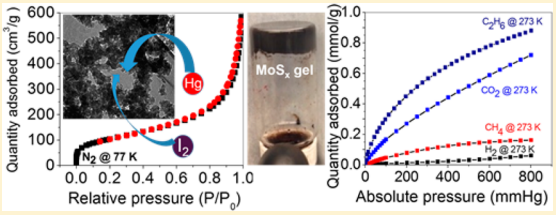

INTRODUCTION

Aerogels are three-dimensional porous materials with low density, highly accessible nanoscale pores, and inherently high surface area.[1] They are mostly empty space and are composed of randomly interconnected nanoparticles. The high porosity and high surface area of aerogels render them suitable for unique applications in catalysis,[2] thermal insulation,[3] sensors,[4] and environmental remediation.[5] Generically, gels are prepared by sol−gel routes which produce randomly interconnected three-dimensional networks filled with the solvent liquid. The removal of the solvent, without causing destruction of the gel's pore structure, leads to aerogel.[1] Most common aerogels are either oxides such as silica,[6] other main group and transition metal oxides,[7] or carbon materials.[8] Nonoxidic materials, mainly chalcogenides, can produce unique aerogels of great interest owing to their rich and tunable electronic and redox properties. They feature intrinsic characteristics such as high surface polarizability, soft Lewis basicity, and high surface area.[9] Chalcogenide aerogels can be prepared via three routes: thiolysis,[10] nanoparticle condensation,[11] and metathesis.[12] In metathesis, the gels are obtained by the coordinative reaction of chalcogenide clusters with metal or cluster linkers. Utilizing metathesis approaches, we have prepared chalcogenide gels (chalcogels) from the anionic building blocks $[MQ_4]^{4-}$, $[M_2Q_6]^{4-}$, and $[M_4Q_{10}]^{4-}$ (M = Ge, Sn; Q = S, Se) with platinum metal linkers.[12] The obtained aerogels show band gap values from 0.2 to 2 eV and large internal surface area with broad pore-size distribution. The metathesis chemistry was extended to a wide variety of chalcogenide spacers (MoS_4^{2-}, $Mo_3S_{13}^{2-}$, SnS_4^{4-}, $Sn_2S_6^{4-}$, $Sn_4S_{10}^{4-}$, SbS_3^{3-}, and AsS_3^{3-})[13] including polychalcogenido anions (S_4^{2-}, S_5^{2-}, and S_6^{2-})[14] and different metal linkers such as Ni, Co, Sb, Zn, Pb, and Bi.[15] Because of their high surface area and multifunctional nature, the chalcogels show promising catalytic, gas separation, and environmental remediation properties. For example, the $NiMoS_4$ and $CoMoS_4$ chalcogels have been shown to be more active than conventional catalysts[13a] for hydrodesulfurization (HDS) of thiophene while $CoMo_3S_{13}$ chalcogel exhibits extraordinary selectivity for ethane and carbon dioxide from hydrogen and methane.[13b] FeS- and FeMoS-based biomimetic chalcogels are effective for photocatalysis.[16] FeMoS-based chalcogels are shown to photochemically reduce N_2 to form NH_3 under white light irradiation at ambient conditions.[17] Polysulfide chalcogels obtained from the cross-linkage of Pt^{2+} and S_x^{2-} ligands (x = 3, 4, 5, 6) exhibit high adsorption capacity for mercury, which is superior to any known adsorbent.[14b]

We recently reported the synthesis of molybdenum sulfide chalcogel using molybdenum thiochloride, MoS_2Cl_3.[18] The chalcogel was formed through metathesis reaction between MoS_2Cl_3 and $(NH_4)_2MoS_4$, in which the chlorine anions from MoS_2Cl_3 were exchanged with MoS_4^{2-} linkers and the product polymerized to form the gel. Here we report the synthesis of a new molybdenum sulfide chalcogel from the oxidative coupling of MoS_4^{2-} using iodine. Recent studies have demonstrated that chalcogels show good affinity for iodine $I_2(g)$ as well as Hg vapor. The former is of particular interest to the nuclear energy community in search of finding effective means to capture the

Received: August 27, 2015
Published: October 10, 2015

DOI: 10.1021/jacs.5b09110
J. Am. Chem. Soc. 2015, 137, 13943−13948

long-lived radioactive isotope $^{129}I_2(g)$[19] while the latter is relevant to environmental efforts to effectively remove mercury from emissions derived from coal fired power plants.[14b,20]

Herein, we report a simple and novel strategy to prepare a highly porous MoS_x chalcogel that departs from the metathesis paradigm and utilizes a redox process. We report facile formation of MoS_x chalcogels by treating the MoS_4^{2-} with iodine (see eq 1) followed by supercritical drying. We show that the new chalcogel possesses an inherently large surface area and pores ranging from the meso to macro region. X-ray photoelectron spectroscopy (XPS) and pair distribution function (PDF) analyses suggest that oxidation state of Mo is 4+ and local structure of MoS_x chalcogel is very similar to that of $[Mo_3S_{13}]^{2-}$ cluster. The high surface area, polarizability, visible-light response, and rich S−S network render the MoS_x chalcogel suitable for catalytic and environmental remediation applications. The MoS_x aerogel exhibits highly selective gas adsorption properties. We also utilized the new MoS_x aerogel as an efficient adsorbent of iodine and Hg vapor.

$$(NH_4)_2MoS_4 + I_2 \rightarrow MoS_4 + 2NH_4I \quad (1)$$

RESULTS AND DISCUSSION

Synthesis. To form the gel, 1.2 mmol of iodine dissolved in 2 mL of dimethylformamide (DMF) was slowly added to a solution of 1.2 mmol of ammonium tetrathiomolybdate ($(NH_4)_2MoS_4$) in 4 mL of formamide (FM). The dark red solution of $(NH_4)_2MoS_4$ in FM turned black to give a product on the addition of a violet solution of iodine in DMF. The black pasty product obtained after aging for one month was washed thoroughly with a mixture of water and ethanol followed by ethanol for 10 days. In this process, the product was washed with water and ethanol twice a day for 5 days and finally washed with ethanol twice a day for five more days. The inset in Figure 1a shows a typical image of the gel after washing. In order to obtain a porous aerogel, the washed gel was dried using supercritical CO_2 at 42 °C and a pressure of 1400 psi. This aerogel product appears fluffy and brown-black in color. If the supercritical drying step is not performed and instead the sample is dried by evaporating the solvent, a black solid so-called xerogel is obtained.

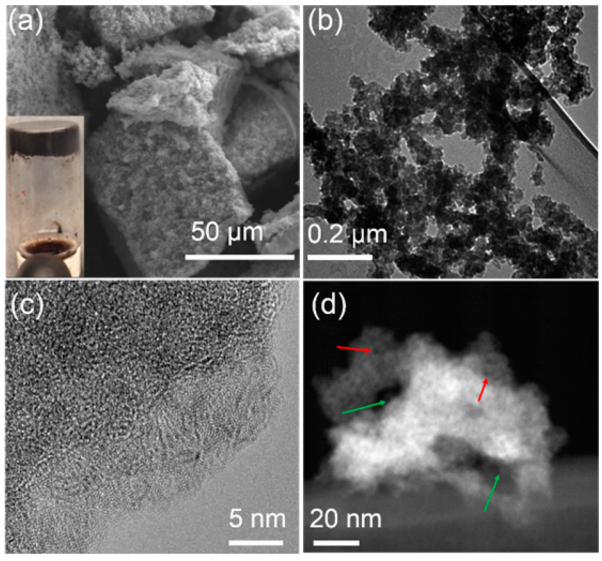

Figure 1. (a) SEM micrograph, (b, c) TEM micrographs, and (d) HAADF-STEM image of MoS_x aerogel. Inset in (a) represents the photograph of MoS_x wet gel.

Characterization. The brown-black chalcogel samples were characterized by scanning electron microscopy (SEM), X-ray diffraction (XRD), transmission electron microscopy (TEM), scanning transmission electron microscopy (STEM), thermogravimetric analysis (TGA), inductively coupled plasma-atomic emission spectroscopy (ICP-AES), and pair distribution function (PDF) analysis. SEM micrographs (Figure 1a) indicate that the aerogel is porous and spongy in nature, whereas xerogel looks nonporous and relatively denser in comparison to its aerogel counterpart (see Figure S1). To investigate the microstructure of the chalcogel, TEM and STEM imaging was performed, and representative images are shown in Figure 1b–d. The TEM micrographs show (Figure 1b,c) the randomly interconnected network of nanoparticles and pores in the range of meso (2−50 nm) and macro (>50 nm) region, which is typical for gel structures. The HAADF (high angle annular dark-field)-STEM image (Figure 1d) shows Z-contrast where porous areas appear darker. The large pores, as shown by the green arrowhead, have size of about 50−100 nm, while the existence of many smaller pores (having dark contrast) are readily observable, as shown by red arrowheads.

The elemental energy dispersive spectroscopy (EDS) data collected from multiple sample locations show the presence of Mo and S in the ratio of 1:3 to 1:4 (Figure S1 in Supporting Information). In order to find the content of any remnant ammonium ion in MoS_x, we treated the MoS_x wet gel with excess of KCl, and the resultant material was analyzed with EDS. From EDS results, the composition of the gel after treating with KCl is found to be $K_{0.03}MoS_4$ (see Figure S2). Therefore, the composition of the MoS_x gel can be written as $(NH_4)_{0.03}MoS_4$; however, for convenience we will refer to it here as MoS_x.

To further raise the ammonium content in the chalcogel network and thereby utilize the chalcogel as an ion-exchange material, we formed the ion-exchangeable gel by treating $(NH_4)_2MoS_4$ with substoichiometric equivalents of iodine. For example, in one experiment, 1.1 mmol of iodine dissolved in 2 mL of DMF was slowly added to 1.2 mmol of $(NH_4)_2MoS_4$ dissolved in 4 mL of FM. The substoichiometric attempts have a limit since lower stoichiometric equivalents of iodine (i.e., 0.5, 0.75, and 0.83 I_2) did not yield a gel. A typical balanced equation for the formation of an ion-exchangeable gel can be written as

$$(NH_4)_2MoS_4 + 0.9I_2 \rightarrow (NH_4)_{0.2}(MoS_4) + 1.8NH_4I \quad (2)$$

As the iodine equivalents are slightly below the stoichiometric ratio, the resultant gel network has an anionic residual charge which is balanced by the NH_4^+ ions. The NH_4^+ ions are located within the pores of the network and can be exchanged with Cs^+ or K^+ ions. EDS analysis of the Cs- and K-exchanged gel evidenced that the NH_4^+ ions in the gel network were readily exchanged with Cs^+ and K^+ ions (Figure S3). This ion-exchange property is important when functionalizing the chalcogel with different cations.

The powder XRD pattern of the MoS_x aerogel is shown in Figure 2a. It predominantly shows the presence of broad diffuse features with the main broad peak centered at ∼45° 2θ. The absence of crystalline peaks infers that the gels are amorphous random networks. To evaluate porosity, the surface areas of

DOI: 10.1021/jacs.5b09110
J. Am. Chem. Soc. 2015, 137, 13943−13948

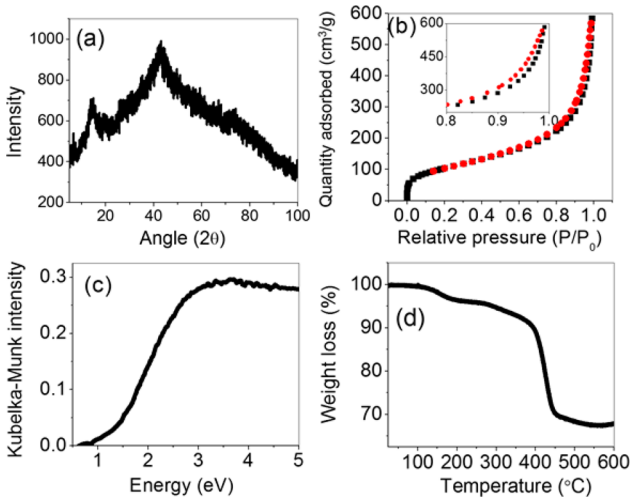

Figure 2. (a) Powder X-ray diffraction pattern, (b) N_2 adsorption and desorption isotherms at 77 K, (c) solid-state UV−vis/NIR optical absorption spectrum (converted from reflectance), and (d) TGA trace of the MoS_x aerogel. Inset in (b) represents the magnified view of the corresponding isotherms at the higher pressure regime showing hysteresis.

aero- and xerogels were determined using the Brunauer−Emmett−Teller (BET) model and N_2 adsorption data at 77 K. The analysis showed that the aerogels exhibit type II isotherms (Figure 2b) with high specific surface areas ranging from 115 to 370 m^2/g, which correspond to the silica equivalent surface areas of 275−890 m^2/g. The obtained silica equivalent surface areas are comparable to highly porous silica aerogels prepared by wet methods. The small so-called H3 hysteresis loop observed at the high pressure regime (inset in Figure 2b) could be attributed to pore blocking (percolation) effects.[21] Barrett−Joyner−Halenda (BJH) analysis of the sorption data indicated a broad range of pores confirming the aerogel nature. The BJH adsorption and desorption average pore diameters are 12 and 10 nm, respectively. The xerogel version, obtained by vacuum drying of the wet gel, shows almost negligible porosity (BET surface area ~0.2 m^2/g), indicating the destruction of pore structure during evaporation of solvents. Figure 2c depicts the UV−vis/NIR spectrum of MoS_x chalcogel. It reveals that the MoS_x chalcogel absorbs light in the entire visible region with a band gap of 1.36 eV (912 nm), raising the possibility in uses as photoelectrode material. The infrared spectrum obtained from the MoS_x chalcogel (Figure S4a) exhibits broad bands between 500 and 570 cm^{-1}, which are attributed to S−S stretching modes of S_2^{2-} moieties in the chalcogel.[22]

In order to assess the thermal stability, TGA of the MoS_x chalcogel was carried out under a nitrogen atmosphere with a heating rate of 10 °C/min in the temperature range of 25−600 °C. Figure 2d shows the TGA trace of MoS_x aerogel. Two stages of weight loss up to 10 and 20 wt % were observed around 200 and at 400 °C, respectively. The weight loss below 200 °C corresponds to liberation of residual solvent left from the synthesis of gel. The sharp drop at 450 °C can be attributed to the decomposition of MoS_x. Powder X-ray diffraction of the final product shows crystalline peaks of MoS_2 (Figure S4b). In addition, EDS analysis of the decomposed product showed the presence of Mo and S in a 1:2 ratio, confirming the formation of MoS_2 compound (see Figure S5). These results are in agreement with the reported thermal decomposition of amorphous MoS_3 to MoS_2.[23]

PDF data from a MoS_x aerogel collected at room temperature show atomic correlations up only to ~5 Å (Figure 3a), which is consistent with the nonperiodic nature of the

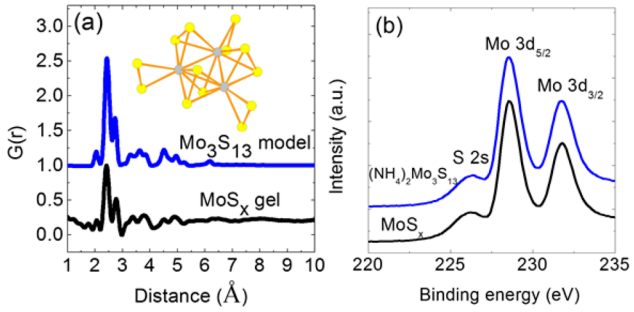

Figure 3. (a) Comparison plot of experimental PDF of MoS_x chalcogel and calculated PDF from a Mo_3S_{13} cluster. (b) High-resolution Mo $3d_{5/2}$ and $3d_{3/2}$ and S 2s XPS spectra of MoS_x chalcogel and $(NH_4)_2Mo_3S_{13}$ crystalline standard. Inset in (a) depicts the structure of the $[Mo_3S_{13}]^{2-}$ unit.

chalcogels but implying a well-defined local short-range order. Modeling of the PDF data indicates that MoS_x primarily consists of $[Mo_3S_{13}]$-like building blocks with triangular Mo metal clusters surrounded by sulfur atoms such as the one found in $(NH_4)_2Mo_3S_{13}$.[24] The comparison of experimental PDF of MoS_x chalcogel and calculated PDF from a Mo_3S_{13} cluster can be seen in Figure 3a. The local structure of MoS_x contains S−S (~2.1 Å), Mo−S (~2.4 Å), and Mo−Mo (~2.8 Å) interactions similar to those of Mo_3S_{13} clusters. Interestingly, the MoS_x chalcogel does not consist of a random arrangement of interconnected MoS_4 building blocks despite the fact we used a MoS_4-containing precursor ($(NH_4)_2MoS_4$). Any arrangement of MoS_4 tetrahedra is expected to give PDF peaks at around ~2.2 Å (Mo−S) and ~3.6 Å (S−S) (Figure S6), peaks that are very weak in the experimental PDF data which may suggest a small concentration of MoS_4 units. XPS data showed that all Mo atoms in the chalcogels are Mo^{4+} showing Mo $3d_{5/2}$ and $3d_{3/2}$ core-level signals with binding energy at 228.6 and 231.8 eV, respectively, which match the oxidation state of Mo in Mo_3S_{13} (Figure 3b). It is noteworthy that the oxidation of a $[MoS_4]^{2-}$ cluster, in which Mo^{6+} species exist, results in a compound where the Mo is reduced to 4+. This is a known characteristic of thiomolybdate chemistry where the high oxidation state of Mo^{6+} is destabilized as the negative charge on the ligands is lowered. The first documented example of such chemistry was found in the oxidation of $[MoS_4]^{2-}$ with S_8 resulting in $[MoS_9]^{2-}$, where a reduced Mo^{4+} ion is coordinated with S_4^{2-} ligands.[25]

Gas Adsorption and Selectivity. The porous nature and high polarizable internal pore surface of the MoS_x chalcogel prompted us to investigate the adsorption properties with H_2, CO_2, CH_4, and C_2H_6. In Figure 4a, we show the adsorption equilibrium isotherms of MoS_x aerogel for H_2, CO_2, CH_4, and C_2H_6 at 273 K. Among the examined gases, C_2H_6 and CO_2 exhibit the highest adsorption. The observed high affinity for C_2H_6 and CO_2 over H_2 and CH_4 can be attributed to the more polarizable C_2H_6 and CO_2 molecules over H_2 and CH_4; the polarizability order is $C_2H_6 > CO_2 > CH_4 > H_2$.[26] Applying the ideal adsorbed solution theory (IAST)[27] model to the single-component isotherms of C_2H_6, CO_2, CH_4, and H_2 at 273 K, the C_2H_6/H_2, CO_2/H_2, and CH_4/H_2 selectivities were calculated. For the pairs C_2H_6/H_2 and CO_2/H_2, the MoS_x aerogel

DOI: 10.1021/jacs.5b09110
J. Am. Chem. Soc. 2015, 137, 13943−13948

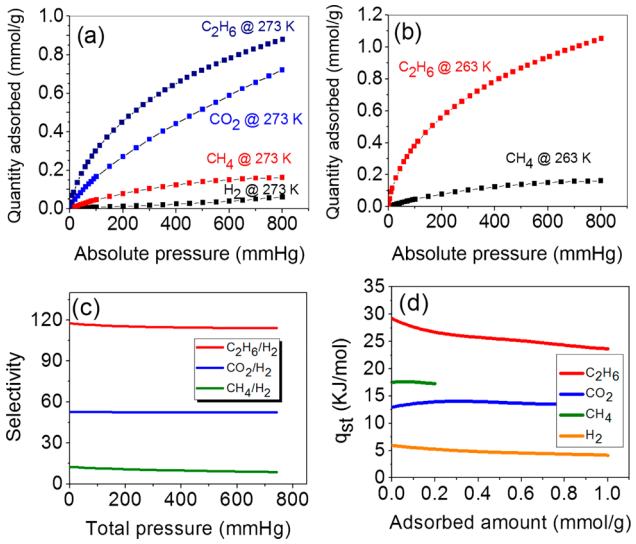

Figure 4. (a) Adsorption isotherms for H_2, CO_2, CH_4, and C_2H_6 of the MoS_x aerogel at 273 K. (b) Ethane (C_2H_6) and methane (CH_4) adsorption isotherms of MoS_x aerogel at 263 K as a function of pressure. (c) Calculated C_2H_6/H_2, CO_2/H_2, and CH_4/H_2 selectivities according to the IAST model. (d) Loading dependence of isosteric heat of adsorption for C_2H_6, CO_2, CH_4, and H_2 of the MoS_x aerogel.

exhibited an almost pressure independent selectivity profile with high separation factors up to ~118−114 and 53−52, respectively (Figure 4c). The selectivity profile for CH_4/H_2 is weekly pressure dependent and showed a separation factor of ~12 in the low-pressure limit. The selectivities for C_2H_6/H_2 and CO_2/H_2 are similar to those obtained in the case of $CoMo_3S_{13}$ chalcogel and compare higher than those of carbons,[28] zeolites,[29] and any other chalcogel.[13a,15,30]

To determine the isosteric heat of adsorption (q_{st}), we also performed adsorption experiments at different temperatures. Figure 4b and Figure S7a,b depict the adsorption equilibrium isotherms of MoS_x aerogel for C_2H_6 and CH_4 at 263 K, H_2 at 77 and 87 K, and CO_2 at 263 and 273 K, respectively. At the limit of zero coverage, the MoS_x aerogel exhibited isosteric heat of adsorptions of about 29, 13, and 6 kJ/mol for C_2H_6, CO_2, and H_2, respectively (Figure 4d). The q_{st} value for CH_4, at the limit of zero coverage, was estimated to be ~17 kJ/mol. The observed heats of adsorption for C_2H_6, CO_2, and H_2 in MoS_x chalcogel are in very good agreement with the determined q_{st} values for the $CoMo_3S_{13}$ chalcogel[13b] and mesoporous germanium-rich chalcogenide frameworks.[31] The isosteric heat of adsorption for hydrogen matches those of other chalcogels (Ni/Co/Ni−Pd/Co−Pd)MoS_4,[13a,15] supporting the nonpreferential adsorption of hydrogen on the polarizable chalcogel surface. These q_{st} values infer that the adsorption interactions between the adsorbate molecules and the specific chalcogenide surface devolve on the polarizability of adsorbate, and enthalpy of adsorption increases with increasing the polarizability of adsorbed molecules. Based on the selective adsorption of gases and isosteric heat of adsorption calculations, MoS_x chalcogel can have important implications in gas separations especially for hydrogen purification processes.

Capture of Iodine and Mercury. The MoS_x aerogel was also tested for iodine and mercury uptake experiments that were carried out in a nitrogen-filled glovebox as reported elsewhere.[14b,19c] Commercially obtained high-purity (Sigma-Aldrich, ≥99.8%) nonradioactive iodine and mercury solids were employed. In a typical experiment, a precisely weighted MoS_x sample (20−100 mg) was placed in a conical-shaped filter paper, which was attached at the top of the glass vial, and an amount of 100−600 mg iodine (or mercury) was placed at the bottom of the vial. This setup was placed in another larger vial that was kept in a sand bath. The temperature of the sand bath was maintained at 60 and 140 °C for iodine and mercury adsorption testing, respectively. After completion of adsorption (within ~24 h), the iodine and mercury loaded chalcogels were transferred from the filter paper and weighed. The MoS_x aerogel showed high iodine and mercury uptake, reaching up to 100 mass % (1 g/g) and 200 mass % (2 g/g), respectively, as revealed by the difference in weight of chalcogels before and after adsorption.

The iodine uptake values are comparable to those of NiMoS, CoMoS, SbSnS, and ZnSnS chalcogels,[18c] metal−organic framework ZIF-8,[32] and layered double hydroxides intercalated with polysulfides.[33] The obtained high iodine uptake capacity implies that the MoS_x chalcogel has a high potential to act as a host matrix for capturing radioactive iodine (I-131).[19c,34] The mercury uptake values are very high and comparable to those of platinum polysulfide chalcogels[14b] and larger than those of any other materials reported to date including polysulfide intercalated layered double hydroxides,[20c] sulfur impregnated coal,[35] sulfur functionalized activated fibers,[36] phenolic polymers,[35] Fe/Cu−S nanoaggregates,[37] and sulfur functionalized copper-doped porous silica.[38] The presence of high porosity of the aerogel facilitates the diffusion of adsorbate throughout the porous structure, leading to high uptake of iodine and mercury. As a result, the pristine MoS_x aerogel became relatively dense after adsorption.

The iodine and mercury loaded samples were examined with XRD, TGA, SEM-EDS, and ICP-AES analyses. The XRD patterns of iodine and mercury loaded chalcogels revealed that the former was amorphous whereas the latter had developed Bragg diffraction peaks that were indexed to HgS (Figure S8a). In order to understand the nature of iodine binding, TGA of iodine-loaded chalcogels was carried out. The iodine-loaded MoS_x showed major mass loss up to 50% in the 75−300 °C temperature range and showed up to 20% mass loss after 300 °C exhibiting a similar trend as its pristine counterpart (Figure S8b). The mass loss below 300 °C can be ascribed to the release of weakly physisorbed molecular iodine on the chalcogel surface. From the above observations, it appears that Hg chemically reacted with MoS_x to form the metal sulfide HgS, whereas iodine did not appear to undergo a chemical reaction as formation of iodide complexes was not observed after iodine adsorption.

To determine the presence and content of iodine and mercury in the chalcogels, both the iodine and mercury loaded MoS_x samples were analyzed by EDS. The SEM micrographs and EDS data of the iodine and mercury loaded samples are shown in Figure S9. The locations from where the EDS spectra were obtained are marked in the respective micrographs. After adsorption of iodine and mercury, the chalcogels appeared to be relatively nonporous. EDS data showed that the iodine and mercury loaded samples contained ~50 and ~66 wt % of I_2 and Hg loading which correspond to 100 and 200 wt % of uptake values, respectively. ICP-AES analysis further confirmed the Hg uptake value estimated from the EDS spectra and showed that the composition of mercury loaded sample was approximately $Hg_{1.9}MoS_4$. The iodine uptake determined by EDS analysis and

DOI: 10.1021/jacs.5b09110
J. Am. Chem. Soc. 2015, 137, 13943−13948

mercury uptake determined from EDS and ICP analyses are consistent with those obtained from the mass difference of the chalcogels before and after adsorption of iodine and mercury.

The high uptake of iodine by the MoS_x aerogel is attributed to the soft polarizable Mo−S surface in the gel network. This favors the physisorption of iodine which is also soft and polarizable through soft acid−soft base interactions.[19a,39] The high adsorption capacity of MoS_x aerogel for Hg vapor can be attributed to the S−S bonding sites in the chalcogel structure which allows the oxidative insertion of the Hg atom to form S−Hg−S units.[14b] The balanced chemical equation for the chemisorption of Hg can be written as

$$-S-S- + Hg \rightarrow -S-Hg-S- \quad (3)$$

In addition to chemisorption, there is also a possibility that Hg undergoes physisorption on the porous chalcogel network.

CONCLUSIONS

A new high-surface-area porous molybdenum sulfide aerogel was prepared from oxidative coupling of ammonium tetrathiomolybdate using iodine. The gel network comprises $[Mo_3S_{13}]$-like building blocks with a formal charge of molybdenum of 4+. The chalcogel exhibits high BET surface area up to 370 m^2/g and selectively adsorbs H_2, CO_2, CH_4, and C_2H_6 gases based on their polarizability. Owing to the preferential adsorption of gases, the MoS_x aerogel is promising for use in gas separations. The selectivity in gas adsorption can be further enhanced by increasing the soft nature of chalcogel network. Given the catalytic importance of the molybdenum sulfides, having adsorption in the visible region, the present porous MoS_x aerogel may have implications in hydrodesulfurization (HDS) and photocatalysis. The MoS_x aerogel is shown to be a promising host matrix for capturing iodine and mercury vapor, processes of interest to the nuclear energy industry and to environmental remediation associated with coal-fired power plants, respectively. The ability to uptake mercury is due to chemical reactivity through chemisorption and the high specific surface area of the chalcogels whereas iodine uptake is mainly due to only physisorption.

ASSOCIATED CONTENT

Supporting Information

The Supporting Information is available free of charge on the ACS Publications website at DOI: 10.1021/jacs.5b09110.

Preparation of $(NH_4)_2MoS_4$, ion-exchange experiments, characterization of chalcogels (PDF)

AUTHOR INFORMATION

Corresponding Author

*E-mail m-kanatzidis@northwestern.edu.

Notes

The authors declare no competing financial interest.

ACKNOWLEDGMENTS

This research was supported by a NEUP grant from the Department of Energy, Office of Nuclear Energy. Support from the UOP Company is also acknowledged. K.S.S. acknowledges the Indo-US Science & Technology Forum (IUSSTF) for a postdoctoral fellowship. SEM, TEM, and XPS were performed at the EPIC facility of the NUANCE Center at Northwestern University. The NUANCE Center is supported by NSF-NSEC, NSF-MRSEC, the Keck Foundation, the State of Illinois, and Northwestern University. ICP-AES was performed at IMSERC in Northwestern University. This research used resources of the Advanced Photon Source, a U.S. Department of Energy (DOE) Office of Science User Facility operated for the DOE Office of Science by Argonne National Laboratory under Contract No. DE-AC02-06CH11357.

REFERENCES

(1) Hüsing, N.; Schubert, U. *Angew. Chem., Int. Ed.* **1998**, *37*, 22.
(2) (a) Rolison, D. R. *Science* **2003**, *299*, 1698. (b) Pajonk, G. M. *Appl. Catal.* **1991**, *72*, 217. (c) Schneider, M.; Baiker, A. *Catal. Today* **1997**, *35*, 339.
(3) Wiener, M.; Reichenauer, G.; Braxmeier, S.; Hemberger, F.; Ebert, H. P. *Int. J. Thermophys.* **2009**, *30*, 1372.
(4) (a) Leventis, N.; Elder, I. A.; Rolison, D. R.; Anderson, M. L.; Merzbacher, C. I. *Chem. Mater.* **1999**, *11*, 2837. (b) Delaizir, G.; Lucas, P.; Zhang, X. H.; Ma, H. L.; Bureau, B.; Lucas, J. *J. Am. Ceram. Soc.* **2007**, *90*, 2073.
(5) Klabunde, K. J.; Richards, R. M. *Nanoscale Materials in Chemistry*; John Wiley & Sons, Inc.: Hoboken, NJ, 2009.
(6) Hench, L. L.; West, J. K. *Chem. Rev.* **1990**, *90*, 33.
(7) Long, J. W.; Rolison, D. R. *Acc. Chem. Res.* **2007**, *40*, 854.
(8) Pekala, R. W. *J. Mater. Sci.* **1989**, *24*, 3221.
(9) Bag, S.; Arachchige, I. U.; Kanatzidis, M. G. *J. Mater. Chem.* **2008**, *18*, 3628.
(10) (a) Allen, G. C.; Paul, M.; Dunleavy, M. *Adv. Mater.* **1992**, *4*, 424. (b) Stanic, V.; Pierre, A. C.; Etsell, T. H.; Mikula, R. J. *J. Non-Cryst. Solids* **1997**, *220*, 58. (c) Stanic, V.; Pierre, A. C.; Etsell, T. H.; Mikula, R. J. *J. Mater. Res.* **1996**, *11*, 363.
(11) (a) Gacoin, T.; Malier, L.; Boilot, J. P. *J. Mater. Chem.* **1997**, *7*, 859. (b) Gacoin, T.; Malier, L.; Boilot, J. P. *Chem. Mater.* **1997**, *9*, 1502.
(12) Bag, S.; Trikalitis, P. N.; Chupas, P. J.; Armatas, G. S.; Kanatzidis, M. G. *Science* **2007**, *317*, 490.
(13) (a) Bag, S.; Gaudette, A. F.; Bussell, M. E.; Kanatzidis, M. G. *Nat. Chem.* **2009**, *1*, 217. (b) Shafaei-Fallah, M.; Rothenberger, A.; Katsoulidis, A. P.; He, J.; Malliakas, C. D.; Kanatzidis, M. G. *Adv. Mater.* **2011**, *23*, 4857. (c) Oh, Y.; Bag, S.; Malliakas, C. D.; Kanatzidis, M. G. *Chem. Mater.* **2011**, *23*, 2447. (d) Ahmed, E.; Rothenberger, A. *Microporous Mesoporous Mater.* **2014**, *199*, 74.
(14) (a) Shafaei-Fallah, M.; He, J. Q.; Rothenberger, A.; Kanatzidis, M. G. *J. Am. Chem. Soc.* **2011**, *133*, 1200. (b) Oh, Y.; Morris, C. D.; Kanatzidis, M. G. *J. Am. Chem. Soc.* **2012**, *134*, 14604.
(15) Polychronopoulou, K.; Malliakas, C. D.; He, J.; Kanatzidis, M. G. *Chem. Mater.* **2012**, *24*, 3380.
(16) (a) Yuhas, B. D.; Smeigh, A. L.; Samuel, A. P. S.; Shim, Y.; Bag, S.; Douvalis, A. P.; Wasielewski, M. R.; Kanatzidis, M. G. *J. Am. Chem. Soc.* **2011**, *133*, 7252. (b) Yuhas, B. D.; Prasittichai, C.; Hupp, J. T.; Kanatzidis, M. G. *J. Am. Chem. Soc.* **2011**, *133*, 15854. (c) Yuhas, B. D.; Smeigh, A. L.; Douvalis, A. P.; Wasielewski, M. R.; Kanatzidis, M. G. *J. Am. Chem. Soc.* **2012**, *134*, 10353. (d) Shim, Y.; Yuhas, B. D.; Dyar, S. M.; Smeigh, A. L.; Douvalis, A. P.; Wasielewski, M. R.; Kanatzidis, M. G. *J. Am. Chem. Soc.* **2013**, *135*, 2330.
(17) Banerjee, A.; Yuhas, B. D.; Margulies, E. A.; Zhang, Y.; Shim, Y.; Wasielewski, M. R.; Kanatzidis, M. G. *J. Am. Chem. Soc.* **2015**, *137*, 2030.
(18) Islam, S. M.; Subrahmanyam, K. S.; Malliakas, C. D.; Kanatzidis, M. G. *Chem. Mater.* **2014**, *26*, 5151.
(19) (a) Riley, B. J.; Chun, J.; Ryan, J. V.; Matyas, J.; Li, X. S.; Matson, D. W.; Sundaram, S. K.; Strachan, D. M.; Vienna, J. D. *RSC Adv.* **2011**, *1*, 1704. (b) Riley, B. J.; Chun, J.; Um, W.; Lepry, W. C.; Matyas, J.; Olszta, M. J.; Li, X.; Polychronopoulou, K.; Kanatzidis, M. G. *Environ. Sci. Technol.* **2013**, *47*, 7540. (c) Subrahmanyam, K. S.; Sarma, D.; Malliakas, C. D.; Polychronopoulou, K.; Riley, B. J.; Pierce, D. A.; Chun, J.; Kanatzidis, M. G. *Chem. Mater.* **2015**, *27*, 2619.
(20) (a) Zheng, Y.; Jensen, A. D.; Windelin, C.; Jensen, F. *Prog. Energy Combust. Sci.* **2012**, *38*, 599. (b) Yee, K.-K.; Reimer, N.; Liu, J.; Cheng, S.-Y.; Yiu, S.-M.; Weber, J.; Stock, N.; Xu, Z. *J. Am. Chem. Soc.*

DOI: 10.1021/jacs.5b09110
J. Am. Chem. Soc. 2015, 137, 13943−13948

2013, *135*, 7795. (c) Ma, S.; Shim, Y.; Islam, S. M.; Subrahmanyam, K. S.; Wang, P.; Li, H.; Wang, S.; Yang, X.; Kanatzidis, M. G. *Chem. Mater.* **2014**, *26*, 5004.
(21) Rouquerol, F.; Rouquerol, J.; Sing, K. *Adsorption by Powders and Porous Solids: Principles, Methodology, and Applications*; Academic Press: San Diego, CA, 1999.
(22) (a) Müller, A.; Sarkar, S.; Bhattacharyya, R. G.; Pohl, S.; Dartmann, M. *Angew. Chem., Int. Ed. Engl.* **1978**, *17*, 535. (b) Fedin, V. P.; Kolesov, B. A.; Mironov, Y. V.; Fedorov, V. Y. *Polyhedron* **1989**, *8*, 2419. (c) Diemann, E.; Müller, A.; Aymonino, P. J. *Z. Anorg. Allg. Chem.* **1981**, *479*, 191.
(23) Weber, T.; Muijsers, J. C.; Niemantsverdriet, J. W. *J. Phys. Chem.* **1995**, *99*, 9194.
(24) Muller, A.; Pohl, S.; Dartmann, M.; Cohen, J. P.; Bennett, J. M.; Kirchner, R. M. *Z. Naturforsch., B: J. Chem. Sci.* **1979**, *34*, 434.
(25) Simhon, E. D.; Baenziger, N. C.; Kanatzidis, M.; Draganjac, M.; Coucouvanis, D. *J. Am. Chem. Soc.* **1981**, *103*, 1218.
(26) Miller, T. M.; Lide, D. R. *Handbook of Chemistry and Physics*; CRC Press: Boca Raton, FL, 2009.
(27) Myers, A. L.; Prausnitz, J. M. *AIChE J.* **1965**, *11*, 121.
(28) Ducrot-Boisgontier, C.; Parmentier, J.; Faour, A.; Patarin, J.; Pirngruber, G. D. *Energy Fuels* **2010**, *24*, 3595.
(29) Belmabkhout, Y.; Sayari, A. *Chem. Eng. Sci.* **2009**, *64*, 3729.
(30) Bag, S.; Kanatzidis, M. G. *J. Am. Chem. Soc.* **2010**, *132*, 14951.
(31) Armatas, G. S.; Kanatzidis, M. G. *Nat. Mater.* **2009**, *8*, 217.
(32) Sava, D. F.; Rodriguez, M. A.; Chapman, K. W.; Chupas, P. J.; Greathouse, J. A.; Crozier, P. S.; Nenoff, T. M. *J. Am. Chem. Soc.* **2011**, *133*, 12398.
(33) Ma, S.; Islam, S. M.; Shim, Y.; Gu, Q.; Wang, P.; Li, H.; Sun, G.; Yang, X.; Kanatzidis, M. G. *Chem. Mater.* **2014**, *26*, 7114.
(34) Carter, J.; Cozzi, A.; Jones, R.; Matthern, G.; Nutt, M.; Priebe, S.; Sorenson, K. Global Nuclear Energy Partnership Integrated Waste Management Strategy, GNEP-WAST-WAST-AI-RT-2008-000214; Savannah River National Laboratory, Aiken, SC, 2008.
(35) Hsi, H. C.; Rood, M. J.; Rostam-Abadi, M.; Chen, S. G.; Chang, R. *J. Environ. Eng. (Reston, VA, U. S.)* **2002**, *128*, 1080.
(36) Hsi, H.-C.; Rood, M. J.; Rostam-Abadi, M.; Chen, S.; Chang, R. *Environ. Sci. Technol.* **2001**, *35*, 2785.
(37) Meyer, D. E.; Sikdar, S. K.; Hutson, N. D.; Bhattacharyya, D. *Energy Fuels* **2007**, *21*, 2688.
(38) Meyer, D. E.; Meeks, N.; Sikdar, S.; Hutson, N. D.; Hua, D.; Bhattacharyya, D. *Energy Fuels* **2008**, *22*, 2290.
(39) Parr, R. G.; Pearson, R. G. *J. Am. Chem. Soc.* **1983**, *105*, 7512.

DOI: 10.1021/jacs.5b09110
J. Am. Chem. Soc. 2015, 137, 13943−13948